Tellus (1994), 46A, 98–112
Printed in Belgium – all rights reserved

TELLUS
ISSN 0280–6495

3D turbulence field on the North-Western European Continental Shelf

By GÉRALDINE P. MARTIN[‡]*, and ERIC J. DELHEZ[‡], *GeoHydrodynamics and Environment Research, University of Liège, Sart Tilman B5, B-4000 Liège, Belgium*

(Manuscript received 23 November 1992; in final form 21 May 1993)

ABSTRACT

The 3-dimensional, non-linear, baroclinic, GHER mathematical model for the study of meso-scale motions (time scale of several hours to several days: tides, storm surges, ...) is described. Particular attention is paid to the turbulent closure based on an evolution equation for the turbulent kinetic energy and a parametric expression of the mixing length (k-model). Appropriate boundary conditions and numerical techniques (mode-splitting, implicity, σ-coordinate system, advection scheme) are described. The model is applied to the simulation of the M_2 tide on the North-Western European Continental Shelf not only without wind but also in typical winter and summer conditions. Large spatial variations of the turbulent kinetic energy appear as a result of the variations of depth and tidal activity around the shelf. These variations are clearly related to the different turbulence regimes observed in summer, with frontal structures separating well-mixed waters from stratified ones. The structure and evolution of the vertical profiles of turbulence variables are described and explained in barotropic and baroclinic conditions, under different wind forcings. The evolution of these profiles at the M_2 tide frequency largely depends on the eccentricity of the tidal ellipse.

1. Introduction

The North-Western European Continental Shelf (NWECS) is composed of the shallow seas surrounding the British Isles. For the purpose of this study, it is further bounded by the 200 m isobath to the West, by the 48°N and 61°N parallels and it includes the Skagerrak and the Kattegat. The efforts to grasp marine processes in this area are numerous. Many works have been devoted to the study of the propagation of the M_2 tide, which originates from the Atlantic and is the dominant tidal component on the shelf. For such investigations, simple barotropic depth-integrated models were used, invoking the great mixing produced by the highly energetic tides and storm surges (e.g., Flather, 1976; Ronday, 1976; Heaps, 1983). Such models turned out to be very effective tools for the simulation and forecast of tides and storm surges elevations and depth-mean currents. Then, with the decrease of computer resource costs, modellers moved to three-dimensional barotropic models. These 3D models are likely to be more accurate than 2D models because they allow the exact computation of the so-called shear-effect and a much more precise evaluation of the bottom stress related to the actual bottom velocity. Besides, together with the introduction of the vertical coordinate they introduced the need for the parameterization of vertical turbulent momentum fluxes and hence the need for a turbulent closure. In the first 3D barotropic models, the turbulent closure was rather rudimentary. It simply consisted in prescribing the vertical profile of the turbulent viscosity according to some laboratory results (the asymptotic law of the wall) and easiness considerations (e.g., Nihoul, 1982). As a next step, the turbulent viscosity was related to the ensemble average velocity amplitude through an algebraic expression (e.g., Davies and Furnes, 1980). When the effects of temperature and salinity

[‡] Research Assistant, FNRS.
* Corresponding author.

gradients were introduced, the turbulent viscosity was made dependent on stratification through the flux Richardson number or the Richardson number (e.g., Backhaus and Hainbucher, 1987).

While hydrodynamic models of the NWECS evolved from 2D barotropic to 3D baroclinic models, more and more refined turbulent closure models were developed for geophysical fluid problems (e.g., Leendertse and Liu, 1978; Lumley, 1978; Mellor and Yamada, 1982; Rodi, 1987; Nihoul et al., 1989). These models helped to understand more and more about turbulence and turbulent exchanges. They are much more complex than the first algebraic models as they can include one evolution equation for each Reynolds stress or differential equations for some of the basic characteristics of the turbulence field (turbulent kinetic energy, turbulence macroscale, dissipation rate of the turbulent kinetic energy...). These schemes are usually classified according to the number of additional evolution equations required to express the turbulent closure.

More and more three-dimensional hydrodynamic baroclinic models using a refined turbulent closure are now being developed around the world (e.g., Blumberg and Mellor, 1987; Beckers, 1991), however, most of the existing hydrodynamical models of the NWECS are still barotropic (Davies and Jones, 1990) or use a simple algebraic turbulent closure (Backhaus and Hainbucher, 1987). While such simplifications seem rather valid for the study of the velocity field, they appear as strong limitations for real applications involving vertical exchanges of scalar constituents. The general distribution of a passive consituent must indeed be much more sensitive to the accurate evaluation of vertical turbulent fluxes than the velocity field whose dynamics results also from a lot of other processes (barotropic and baroclinic pressure gradients, Coriolis force...). By the same token, the fate of scalar quantities is also much more sensitive to stratification and its possible inhibition of vertical exchanges. Therefore, with the final goal of studying vertical exchanges of nutrients and other dissolved matters on the shelf, we have designed a three-dimensional, differential, turbulence model taking into account stratification, tidal activity, real topography and wind influence.

This model is based on the three-dimensional model of the GHER which has already been successfully applied to some other regions (Deleersnijder and Nihoul, 1988; Beckers, 1991). It is now adapted to the study of tidal and wind-induced motions on the NWECS. In the course of this paper, these motions will be called the *mesoscale* circulation as they fall into the spectral window ranging from several hours to several days. However, the term "mesoscale" does not refer here to small baroclinic eddies. In fact most of the processes described are barotropic and are not associated with the baroclinic Rossby radius (which is not resolved by this model). The dynamics of temperature and salinity are taken into account in this model only because they introduce large scale baroclinic features and inhibit vertical turbulent exchanges.

The purpose of this paper is to present the mathematical model with its implementation characteristics and to show the main results obtained about the turbulence field. We will try to understand the horizontal, vertical and temporal variations of the turbulence conditions, leaving the analysis of turbulent transfer of scalar constituents for a future study.

2. Mathematical model

The mesoscale circulation model is based on the well known three-dimensional, non-linear and unsteady equations of the "weather of the sea" sustained by the quasi-hydrostatic and Boussinesq approximations. (Nihoul, 1980; Nihoul et al., 1989)

$$\nabla_{\mathrm{h}} \cdot \boldsymbol{u} + \frac{\partial v_3}{\partial x_3} = 0, \tag{1}$$

$$\frac{\partial \boldsymbol{u}}{\partial t} + \boldsymbol{u} \cdot \nabla_{\mathrm{h}} \boldsymbol{u} + v_3 \frac{\partial \boldsymbol{u}}{\partial x_3} + f \boldsymbol{e}_3 \wedge \boldsymbol{u} = -\nabla_{\mathrm{h}} q + \frac{\partial}{\partial x_3}\left(\tilde{v} \frac{\partial \boldsymbol{u}}{\partial x_3}\right) + \nabla_{\mathrm{h}} \cdot (\boldsymbol{K}_{\mathrm{h}}^{u} \nabla_{\mathrm{h}} \boldsymbol{u}), \tag{2}$$

$$\frac{\partial q}{\partial x_3} = -g \frac{\rho - \rho_0}{\rho_0} = b(T, S), \tag{3}$$

$$q = \frac{p}{\rho_0} + g x_3 + \xi, \tag{4}$$

$$\frac{\partial T}{\partial t}+\boldsymbol{u}\cdot\nabla_{\mathrm{h}}T+v_3\frac{\partial T}{\partial x_3}$$
$$=\frac{\partial}{\partial x_3}\left(\tilde{\lambda}^{\mathrm{T}}\frac{\partial T}{\partial x_3}\right)+\nabla_{\mathrm{h}}\cdot(\boldsymbol{K}_{\mathrm{h}}^{\mathrm{T}}\nabla_{\mathrm{h}}T), \tag{5}$$

$$\frac{\partial S}{\partial t}+\boldsymbol{u}\cdot\nabla_{\mathrm{h}}S+v_3\frac{\partial S}{\partial x_3}$$
$$=\frac{\partial}{\partial x_3}\left(\tilde{\lambda}^{\mathrm{S}}\frac{\partial S}{\partial x_3}\right)+\nabla_{\mathrm{h}}\cdot(\boldsymbol{K}_{\mathrm{h}}^{\mathrm{S}}\nabla_{\mathrm{h}}S), \tag{6}$$

where:

$$\nabla=\nabla_{\mathrm{h}}+\frac{\partial}{\partial x_3}\boldsymbol{e}_3$$

the $\boldsymbol{e}_3$ axis is vertical upwards, x_3 [m] denotes the height above the reference level, $\boldsymbol{u}$ [m s^{-1}] is the horizontal velocity vector, v_3 [m s^{-1}] is the vertical component of the velocity vector, f [s^{-1}] is the Coriolis parameter depending on latitude, q [m^2 s^{-2}] is the so-called generalized pressure, g [$=9.81$ m s^{-2}] is the acceleration of gravity, p [kg m^{-1} s^{-2}] is the pressure, ρ [kg m^{-3}] is the density of seawater, ρ_0 is a constant reference value of ρ, ξ [m^2 s^{-2}] is the tidal potential per unit mass, b [m s^{-2}], the buoyancy, is related to stratification and is primarily a function of the temperature T [°C] and the salinity S [°/$_{oo}$] of seawater through the state equation, $\boldsymbol{K}_{\mathrm{h}}$ are isotropic diffusive tensors whose diagonal value is set to 500 m^2 s^{-1} and anticipates the horizontal sub-grid scale non-linear interactions arising from the further domain discretization (Nihoul et al., 1989).

In these equations, the turbulent viscosity, $\tilde{\nu}$ [m^2 s^{-1}], and the turbulent diffusivities of scalar quantities, $\tilde{\lambda}^y$ [m^2 s^{-1}], must be known to close the system. The turbulent closure is performed through a single equation for the turbulent kinetic energy per unit mass, k [m^2 s^{-2}], and an algebraic expression of the mixing length, l [m]. This closure has the great advantage to take into account the advection, the diffusion, the local production-destruction and the history of turbulence through the widely accepted eq. (7) for k. Moreover, sound empirical formulas are available for l in shallow shelf seas (Nihoul, 1984) so that the resolution of a differential equation for ε [m^2 s^{-3}], the dissipation rate of k, can be avoided and replaced by an algebraic expression of the mixing length. The differential equation for ε or for the turbulence macroscale is indeed, by common consent, the weakest point of all turbulent closure schemes. It is therefore perhaps advisable to avoid the additional complexity introduced by a differential equation for one of these quantities by using an algebraic equation for l (eqs. (11) and (12)) which also suffers from important shortcomings but is much less demanding in computer resources.

The values of ε and $\tilde{\nu}$ are then obtained using simple dimensional arguments from the basic variables of the turbulence scheme (eqs. (10) and (13)). The importance of stratification is measured by the flux Richardson number R_{f} (eq. (9)) which appears naturally in the production-destruction term of turbulent kinetic energy (eq. (8)) and seems thus the appropriate controlling factor to parameterize the inhibition of turbulence. Turbulent diffusivities for scalar quantities are supposed to be proportional to the turbulent viscosity $\tilde{\nu}$ according to the Reynolds analogy (eq. (14)). The β^y coefficients are also function of R_{f} because the momentum exchange, involving pressure forces, is likely to maintain its efficiency at high Richardson numbers whereas the transfer of the scalar quantities T, S and b is reduced as stratification increases (Nihoul et al., 1989):

$$\frac{\partial k}{\partial t}+\boldsymbol{u}\cdot\nabla_{\mathrm{h}}k+v_3\frac{\partial k}{\partial x_3}$$
$$=\frac{\partial}{\partial x_3}\left(\tilde{\lambda}^{k}\frac{\partial k}{\partial x_3}\right)+\nabla_{\mathrm{h}}\cdot(\boldsymbol{K}_{\mathrm{h}}^{k}\nabla_{\mathrm{h}}k)+Q^k, \tag{7}$$

$$Q^k=\tilde{\nu}\left\|\frac{\partial\boldsymbol{u}}{\partial x_3}\right\|^2-\tilde{\lambda}^b\left|\frac{\partial b}{\partial x_3}\right|-\varepsilon$$
$$=\tilde{\nu}\left\|\frac{\partial\boldsymbol{u}}{\partial x_3}\right\|^2(1-R_{\mathrm{f}})-\varepsilon, \tag{8}$$

$$R_{\mathrm{f}}=\frac{\tilde{\lambda}^b\left|\dfrac{\partial b}{\partial x_3}\right|}{\tilde{\nu}\left\|\dfrac{\partial\boldsymbol{u}}{\partial x_3}\right\|^2}, \tag{9}$$

$$\varepsilon=k^{3/2}/8l, \tag{10}$$

$$l=l_n(1-R_{\mathrm{f}}), \tag{11}$$

$$l_n=\kappa z\left(1-\delta\frac{z}{H}\right), \tag{12}$$

$$\tilde{\nu} = 0.5 l \sqrt{k} \tag{13}$$

$$\tilde{\lambda}^y = \beta^y \tilde{\nu}, \qquad \beta^k = 1,$$

$$\beta^{\mathrm{T}} = \beta^{\mathrm{S}} = \beta^b = 1.1 \sqrt{1 - R_{\mathrm{f}}} \tag{14}$$

The mixing length l is expressed as the product of the mixing length in neutral stability conditions ($R_{\mathrm{f}} = 0$) and of a decreasing function of the flux Richardson number in conditions of stable stratification. The mixing length profile (Nihoul, 1984) respects the well-established asymptotic boundary layer law $l_n = \kappa \cdot z$ for $z \ll H$ (where the Von Karman constant $\kappa = 0.4$, z is the height measured above the bottom and H is the total depth). At the surface, the parameter $\delta \in [0.5, 1]$ enables the adjustment of the mixing length to wind-mixed layer conditions. Notice that eq. (12) is not valid in the not very extended deeper parts of the domain so that a reasonable upper-limit of 20 m is imposed to the mixing length.

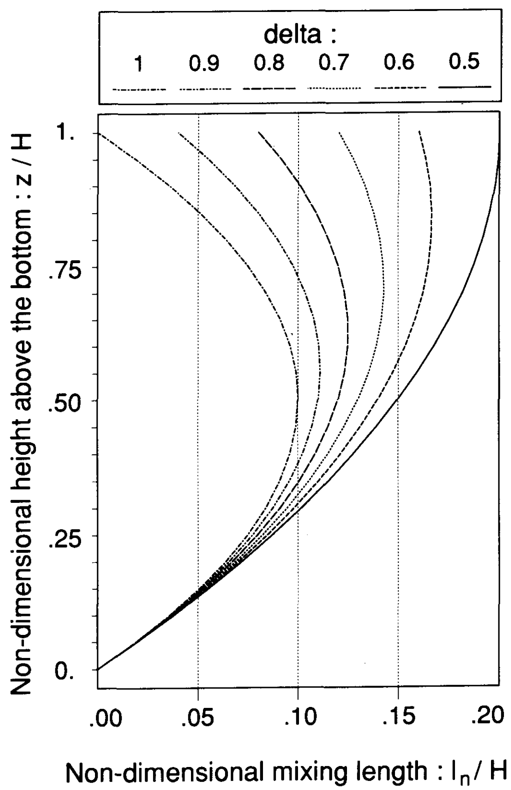

Fig. 1. Non-dimensional mixing length l_n/H versus z/H for different values of the parameter δ.

Preliminary tests have been carried out to study the sensitivity of the results to the value of δ, i.e., to the actual mixing length profile. Fig. 1 shows the non-dimensional mixing length (l_n/H) versus the non-dimensional height above the bottom (z/H) for different values of the parameter δ. It should be noticed that the velocity profiles don't show any appreciable dependence on δ, as long as the asymptotic linear behaviour of the mixing length in the bottom boundary layer is included, except when $\delta = 1$. This borderline case corresponds to an ice-covered sea where the surface layer is exactly identical to the bottom layer. It should thus be rejected here as any other formulation of the mixing length vanishing at the surface. For all other values of δ sufficiently different from 1., the more important sensitivity is of course found by the turbulent viscosity and turbulent kinetic energy profiles, but not by the currents.

Even in the case of negligible wind, the free surface is disrupted by small amplitude wave motions so that the mixing length (the length scale of the energy containing eddies) doesn't vanish at the surface. This results in the turbulent diffusion of turbulence from the core of the water column towards the surface. One must then be very attentive as, with zero wind velocity, the surface turbulent kinetic energy is largely dependent on that turbulent flux and ultimately on δ: it can even double when passing from $\delta = 0.9$ to $\delta = 0.5$! However, in this case of negligible wind, maximum values of k and $\tilde{\nu}$ are found respectively at the bottom and around mid-depth whatever be the value of δ.

When a significant wind is blowing over the surface, the mixing-length at the surface should increase as larger surface oscillations are expected. Thus, a smaller value of δ should be used.

As a consequence of this discussion, δ was set to 0.7 in our simulations running in typical summer conditions of weak wind (or without wind forcing) while it was decreased to 0.5 with stronger winter winds. However, the choice of the appropriate value should remain part of the calibration of the model if experimental field measurements were available. A direct dependence of the parameter δ on the actual wind velocity could also be considered as a possible extension.

3. Boundary conditions

A transformation of the vertical coordinate is performed to obtain a domain characterized by a constant depth with regard to time and to horizontal coordinates instead of the real domain. Let the new vertical coordinate be:

$$\sigma = \frac{x_3 + h}{H}. \tag{15}$$

This transformation allows a simple and efficient management of the memory cells as well as a more precise representation of the bathymetric effects. As a result of the σ-transform, the domain extends vertically from $\sigma = 0$ at the bottom $(x_3 = -h)$ to $\sigma = 1$ at the surface $(x_3 = \zeta$, the free surface elevation). The vertical discretization is achieved through ten levels on each vertical. The vertical increment $\Delta\sigma$ varies to get a finer resolution near the surface and the bottom. A very interesting aspect of this σ-transform is that only one distribution is to be chosen for the whole domain because the real levels thicknesses $(\Delta x_3 = H\,\Delta\sigma)$ automatically adapt themselves to the local depth. The precise resolution of the bottom boundary layer would require a very large number of vertical levels, as shown by Davies and Jones (1990). However, if the first level $\Delta\sigma$ at the bottom is chosen to be in the logarithmic bottom boundary layer in the largest part of the domain, the effect of this layer can be easily and economically parameterized with the following bottom stress expression:

$$\boldsymbol{\tau}_b = \tilde{\nu}\,\frac{\partial \boldsymbol{u}}{\partial x_3} = C_D\,\|\boldsymbol{u}_b\|\,\boldsymbol{u}_b, \tag{16}$$

$$C_D = \left(\frac{\kappa}{\ln(z_b/z_0)}\right)^2, \tag{17}$$

where z_b is the height above the bottom at which the $\boldsymbol{u}_b$ velocity is computed in the bottom mesh and z_0 is the rugosity length $(=3\cdot 10^{-3}\,\mathrm{m})$. In those places where the bottom boundary layer is not well resolved (Norwegian Trench, Skagerrak), it is more appropriate to specify $C_D = 0.0025$. The actual agorithm is to set C_D to the larger of the 2 values given by eq. (17) and 0.0025 (Blumberg and Mellor, 1987). To complete this parameterization, the turbulent kinetic energy value resulting from a local equilibrium of the turbulence in the bottom boundary layer is prescribed at the bottom as in the Blumberg and Mellor's model (Blumberg and Mellor, 1987):

$$k_b = \frac{\|\boldsymbol{\tau}_b\|}{0.25}, \tag{18}$$

whereas the diffusive fluxes of temperature and salinity vanish.

At the air-sea interface, turbulent fluxes are parameterized globally in terms of the classical meteorological variables measured at the reference height of 10 m above the sea level:

$$\tilde{\nu}\,\frac{\partial \boldsymbol{u}}{\partial x_3} = \frac{\rho_{\mathrm{air}}}{\rho_0}\,C_W\,\|\boldsymbol{W}_{10}\|\,\boldsymbol{W}_{10}, \tag{19}$$

$$\tilde{\lambda}^k\,\frac{\partial k}{\partial x_3} = \frac{\rho_{\mathrm{air}}}{\rho_0}\,C_E\,\|\boldsymbol{W}_{10}\|^3, \tag{20}$$

where $\rho_{\mathrm{air}} = 1.29\ \mathrm{kg\,m^{-3}}$, C_W $(=1.456\cdot 10^{-3})$ and C_E $(=0.63\cdot 10^{-6})$ are exchange coefficients and $\boldsymbol{W}_{10}$ is the wind velocity measured at 10 m. Without wind, there is no turbulent flux through the sea surface. On the other hand, when the wind is blowing over the sea, breaking waves inject turbulence in the water column as modelled by eq. (20). Notice that the assumption of the local equilibrium of turbulence used to derive the bottom value of the turbulent kinetic energy (eq. (18)) is not valid in the surface layer. In fact, because of non-zero vertical turbulent diffusivity of turbulent kinetic energy near the surface, the actual turbulent level reached in the surface boundary layer depends not only on wind conditions but also on what happens below. Adequate salinity and heat fluxes must also be imposed at the air-sea interface (Nihoul, 1984).

The correct specification of conditions at open boundaries is still a difficulty in modelling continental shelf circulation. As we focus on mesoscale circulation, we must impose "mesoscale conditions". These mainly consist in the tidal forcing as we do not impose any external storm surge forcing at the open boundary. The model is then driven along its open boundary by tidal variations of the sea surface elevation. The simplest way to impose this elevation is to use a clamped boundary. The elevation associated with the M_2 tide wave is then prescribed as follows:

$$\zeta(s, t) = \mathrm{Amp}_{M_2}(s) \cdot \cos(\omega_{M_2} t - \mathrm{Phas}_{M_2}(s)), \quad (21)$$

where Amp_{M_2} and Phas_{M_2} are the amplitude and phase of the M_2 elevation depending on the position s along the open boundary and where ω_{M_2} is the angular speed of the M_2 tide wave. There may be some problems when tidal elevations are imposed all along the open boundary (as well to the West where the tide enters the shelf as to the North where it leaves it). Indeed, the features of the outgoing wave result from its propagation on the shelf, from the dissipation in shallow waters, from the influence of bathymetry and topography... as they are represented in the model. The "exit" elevations shouldn't be imposed because one runs the risk that calculated and imposed values conflict with each other. Moreover, when the wind blows over the domain, it generates currents and storm surges that propagate as long waves and reach sooner or later the boundary. This produces, on a clamped boundary, spurious reflexions that may spoil the solution computed inside the domain. As a result, a clamped boundary is not appropriate, particularly if one wants to study winter situations characterized by strong winds. A kind of radiation condition must be applied along the open boundary. This condition must allow disturbances generated inside the studied domain to propagate outwards while it must prescribe the tidal forcing as well. After different tests we have chosen a condition, applied with success by Flather (1976), that prescribes an algebraic relation between the perturbation of the depth-mean current normal to the boundary and the perturbation of the elevation at the same point. This relation supposes that the deviation with regard to the reference M_2 situation propagates outwards as a Kelvin wave for which current and elevation are in the ratio $\sqrt{g/H}$. One thus has:

$$q(s, t) - \bar{q}(s, t) = \sqrt{\frac{g}{H(s, t)}} (\zeta(s, t) - \bar{\zeta}(s, t)), \quad (22)$$

where s is the position along the boundary, q is the normal component of the outward depth-mean current, ζ is the elevation, H is the total local depth. $\bar{\zeta}$ and $\bar{q}$ are the oscillating M_2 free surface elevation and depth-mean current derived from Schwiderski's data (Schwiderski, 1979) and adapted to our domain by an iterative procedure similar to the one used by Flather (1976).

Finally, the vertical structure of currents is assumed not to change across the boundary, i.e., the derivative normal to the boundary of the deviation of the velocity with respect to its depth-averaged value is supposed to vanish. This avoid any spurious vertical motion at the boundary. The material derivatives and horizontal diffusive fluxes of the turbulent kinetic energy are neglected at the open boundary according to the Mellor and Yamada level 2 model (Mellor and Yamada, 1982). Climatological mean temperature and salinity derivatives normal to the open boundary are also prescribed.

4. Numerical aspects

The numerical resolution is achieved through the 3D finite differencing method. The equations are discretized on an Arakawa C-grid (Arakawa and Lamb, 1977). The horizontal mesh size is 10′ in longitude and latitude.

All the spatial derivatives are centered-space discretized except for the advective terms of scalar quantities. A great care must be taken when considering these terms. One of the properties of physical advection that one would like the discretized advection scheme to exhibit is that advection carries information from upstream only. This wouldn't be the case with a centered-space scheme and that is why we use a streamline upwind discretization scheme, well known in the finite elements method. Because upwind amounts to the introduction of artificial diffusive fluxes, the upwind discretization scheme can be implemented by using centered-space finite differences of the advective term together with an artificial horizontal diffusivity tensor $\boldsymbol{K}_h^{\mathrm{artif}}$ that is added to the isotropic one $\boldsymbol{K}_h$. By using an anisotropic tensor one can ensure positivity without introducing any artificial diffusive flux across the stream. The amount of artificial diffusivity is controlled by the magnitude of the gradient of the scalar quantity, r, to be advected.

$$\boldsymbol{K}_{\mathrm{h}}^{\mathrm{artif}}(i, j) = k_{\mathrm{h}}^{\mathrm{artif}} \frac{u_i u_j}{\|\boldsymbol{u}\|^2},$$

$$k_{\mathrm{h}}^{\mathrm{artif}} = \sum_{i=1,2} \frac{\alpha_i u_i \Delta_i}{2}, \tag{23}$$

$$\alpha_i = \min\left(1, \frac{|\partial_i r|}{\nabla_{\mathrm{ref}}}\right),$$

where Δ_i is the grid step in the direction i, ∇_{ref} a reference value for the gradient of the scalar quantity r and ∂_i the derivative in the direction i. For instance, with a flow directed along the reference unit vector $\boldsymbol{e}_1$, the only non-zero component of the artificial viscosity tensor is $\boldsymbol{K}_{\mathrm{h}}^{\mathrm{artif}}(1, 1)$ so that the upwind is indeed introduced along the stream.

To reconcile the stability of the numerical scheme and its computational efficiency, a mode-splitting is performed (Simon, 1974). This consists in resolving 2D depth-integrated equations with a small time-step, Δt, to resolve surface gravity waves and the full set of 3D equations with a much longer time step, ΔT. There is of course a close coupling between the 2D and 3D sets of equations. The free surface elevation obtained from the 2D equations is injected into the 3D ones. These in turn provide vertical profiles and baroclinic features necessary to compute the shear effect, the bottom friction and the baroclinic terms in the 2D equations. However, there may be a tendency for the vertical integral of the 3D velocities to differ from the external mode transport on account of truncation errors. To solve this, the former is replaced by the latter every ΔT seconds.

The mode-splitting method is widely used and well-suited when studying slowly changing situations (e.g., James, 1986; Blumberg and Mellor, 1987; Beckers, 1991) but its application to such an unsteady phenomenon as tide requires much prudence. In fact, the vertical structure varies rather rapidly and the time step ΔT must be small enough to catch these variations. Our simulations run with $\Delta T = 621$ s and $\Delta t = 69$ s. The bottom stress computed during a 3D time step must theoretically be held fixed $(=\tau_{\mathrm{b}}^{2\mathrm{D}})$ during the following nine 2D time steps. Practically, this is potentially dangerous when considering tidal phenomena because, at tide reversal, such a bottom stress would sooner or later accelerate the mean stream instead of going on breaking it. Thus, it is more advisable to consider:

$$\tau_{\mathrm{b}}^{2\mathrm{D}} = C_{\mathrm{D}} \|\boldsymbol{u}_{\mathrm{b}}\| (\hat{\boldsymbol{u}}_{\mathrm{b}} + \boldsymbol{u}_{\mathrm{m}}), \tag{24}$$

where $\boldsymbol{u}_{\mathrm{b}}$ (total bottom layer velocity) and $\hat{\boldsymbol{u}}_{\mathrm{b}}$ (deviation of the bottom velocity from the depth-mean one) are held fixed between two successive 3D time steps and where $\boldsymbol{u}_{\mathrm{m}}$ (depth-mean velocity) varies from one 2D time step to the other.

In the discretized model, time derivatives are simply evaluated by forward differencing, giving us an explicit one-step Euler scheme. In fact, the resolution of a particular equation is done using the most recent values for each variable. For example, if the x_2 momentum equation is resolved after the x_1 momentum equation, the values of u_1 used to compute the Coriolis term in the x_2 momentum equation are the ones that have just been computed. Doing so, the scheme is made partly implicit without resolving any set of algebraic equations. Of course, to keep a kind of balance between the two components of the horizontal transport, we must compute u_1 before u_2 at even time steps and u_2 before u_1 at odd ones. This gives a kind of alternate directions scheme with enhanced stability. However, the vertical advective and diffusive fluxes of the different variables must be treated implicitly for numerical stability. The Thomas algorithm is used to solve the resulting tridiagonal systems.

The bottom stress is very delicate to compute in a tidal model because bottom currents change rapidly in magnitude and direction. We think it is worth using a semi-implicit expression of the bottom stress applied to the 3D mode. In this way, the 3D time-step can summarize what has just happened during the previous 2D time-steps in a much better way:

$$\begin{aligned}\tau_{\mathrm{b}}^{3\mathrm{D}} &= (1 - \mathrm{Ti}) \cdot C_{\mathrm{D}} \|\boldsymbol{u}_{\mathrm{b}}\|^{n\Delta T} \boldsymbol{u}_{\mathrm{b}}^{n\Delta T} \\ &\quad + \mathrm{Ti} \cdot C_{\mathrm{D}} \|\boldsymbol{u}_{\mathrm{b}}\|^{n\Delta T} \boldsymbol{u}_{\mathrm{b}}^{(n+1)\Delta T},\end{aligned} \tag{25}$$

where Ti, the implicity rate, is set to 0.5 and n is the number of the time-step. The need for an adjustment between the vertical integral of the 3D velocities and the external mode transport is also reduced thanks to this precaution.

5. Simulations

In all the simulations, the M_2 tidal forcing is imposed along the open boundary (eq. (22)). On the NWECS, the astronomical tidal force gives only a small direct contribution to observed tides with respect to the response to Atlantic tides entering the shelf along its western boundary. It is therefore neglected ($\xi = 0$ in eq. (4)). The first simulation has been run without wind-forcing by means of a simplified model based on the hypothesis of a constant density of seawater ($\rho = \rho_0$) all over the 3D domain. This barotropic model is derived from the baroclinic one by stating $\rho = \rho_0 \Rightarrow b = 0 \Rightarrow R_f = 0$. The equations for T and S are of course not solved in this case. This model is useful to describe most of the mesoscale phenomena. The good computation of amplitudes and phases of the currents and elevations associated to M_2 on the shelf as well as of the tidal harmonic M_4 generated by non-linear interactions on the shelf allows to be confident in the model (Delhez and Martin, 1992).

Spatial variations of the turbulent kinetic energy are significant (Figs. 2, 3). They reflect the spatial distribution of tidal currents. When comparing Figs. 2, 3, one can see that bottom values are greater than surface ones. This is normal because, without wind, the turbulent kinetic energy is mainly produced by the friction of tidal currents on the rough bottom. The significant variations in the magnitude of the turbulent kinetic energy reflect the different regimes occurring on the shelf. Some regions are well-mixed with intense tidal currents (English Channel, Irish Sea, Southern Bight...) while others are less agitated (large regions of the North Sea, Skagerrak, Celtic Sea...).

Two representative points have been chosen to present the results: point 1 is located in the English Channel (49°55′N, 1°35′W, 50 m depth), point 2

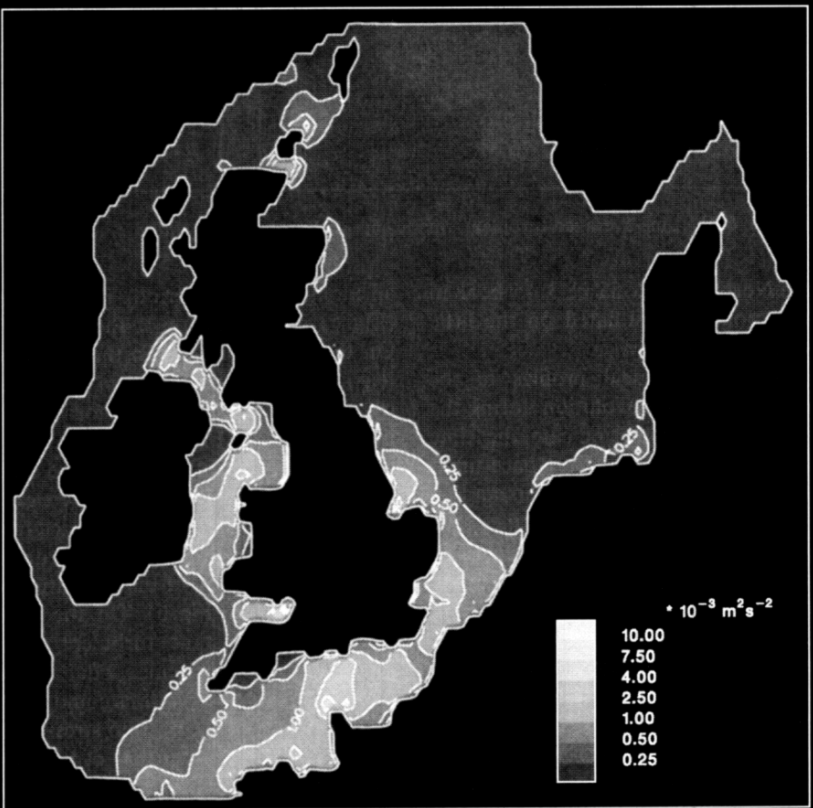

Fig. 2. Surface value of the time-averaged turbulent kinetic energy. Barotropic M_2 tide.

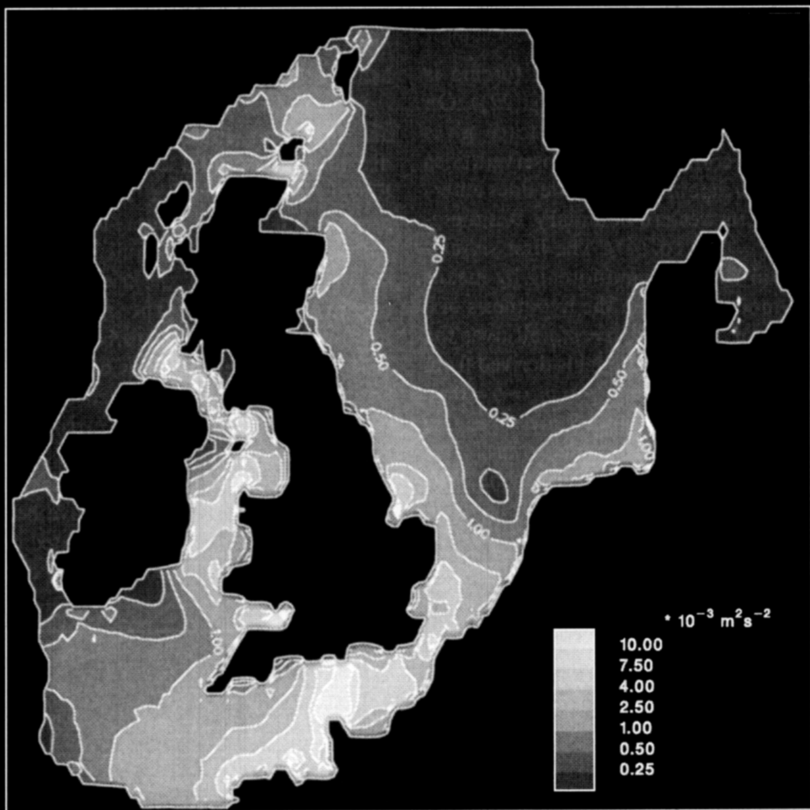

Fig. 3. Bottom value of the time-averaged turbulent kinetic energy. Barotropic M_2 tide.

is located in the North Sea (56°55′N, 3°45′E, 58 m depth). These 2 points are situated on the little maps of Figs. 4, 5, respectively.

Figs. 4, 5 show the vertical profiles of the horizontal velocity and their evolution during the M_2 tidal period. The arrows indicate the time evolution. The original 3D + 1D (space-time) representation allows a very good understanding of the cyclic evolution of the velocity profiles. The phase advance of bottom currents with regard to depth-mean and surface ones can be noticed in the projections of the vertical profiles onto S–N and W–E planes. This is especially apparent at tide reversal of one of the velocity components. At this moment, the magnitude of the velocity vector doesn't necessarily pass through a minimum, as usual 2D-plots of vertical profiles would let us believe. When the eccentricity of the surface tidal ellipse is very low (ellipse nearly circular), the magnitude of the velocity vector is nearly constant all along the tidal period. This is true at point 2 (Fig. 5) representative of the central North Sea. On the other hand, when the eccentricity is high (e.g., along the coasts and in narrow straits), the magnitude of the velocity vector varies a lot during the tidal period (Fig. 4).

The influence of the tidal ellipse eccentricity on the turbulent kinetic energy vertical profiles is also evident. When the eccentricity is high, the magnitude of k varies significantly during the tidal period as a function of the magnitude of the tidal current (point 1, Fig. 6). On the other hand, a much more constant turbulent kinetic energy corresponds to a circular tidal ellipse (point 2, Fig. 7). Similar observations could be stated about the magnitude of the bottom stress and the subsequent possible resuspension of bottom sediments that can exhibit large tidal oscillations or not depending on the tidal ellipse eccentricity. The qualitative aspects of the vertical profiles of k can

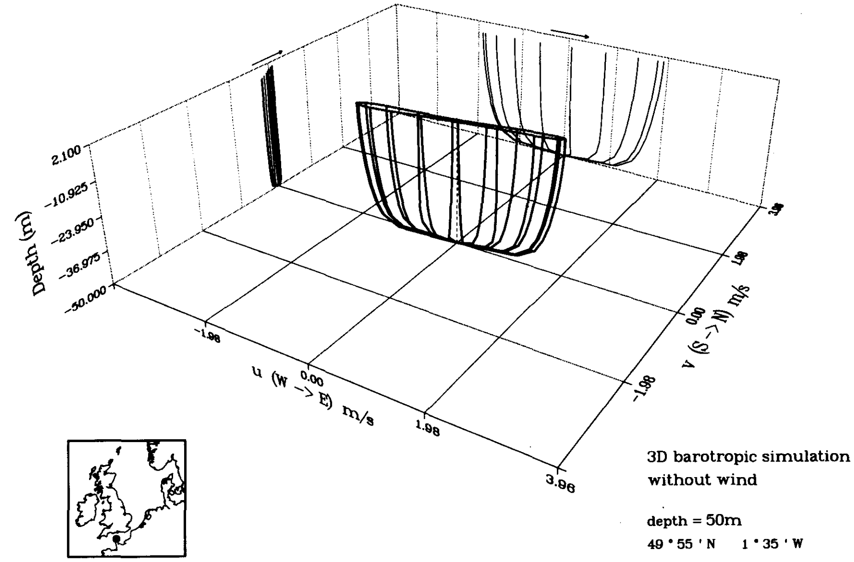

Fig. 4. Evolution of the vertical profile of the horizontal velocity during one M_2 tidal period. Point 1 in the English Channel.

be explained by neglecting horizontal diffusion and advection. This is a reasonable assumption also used in the Mellor and Yamada level 2 model (Mellor and Yamada, 1982). Starting from a low turbulent level, the increase of the bottom friction generates an intensification of the turbulent kinetic energy in the bottom layer. The low starting value of the turbulent viscosity allows only a very low vertical diffusion so that the bottom generated turbulence remains concentrated in the bottom layer (solid lines when bottom turbulence increases, from left to right). When the turbulent kinetic

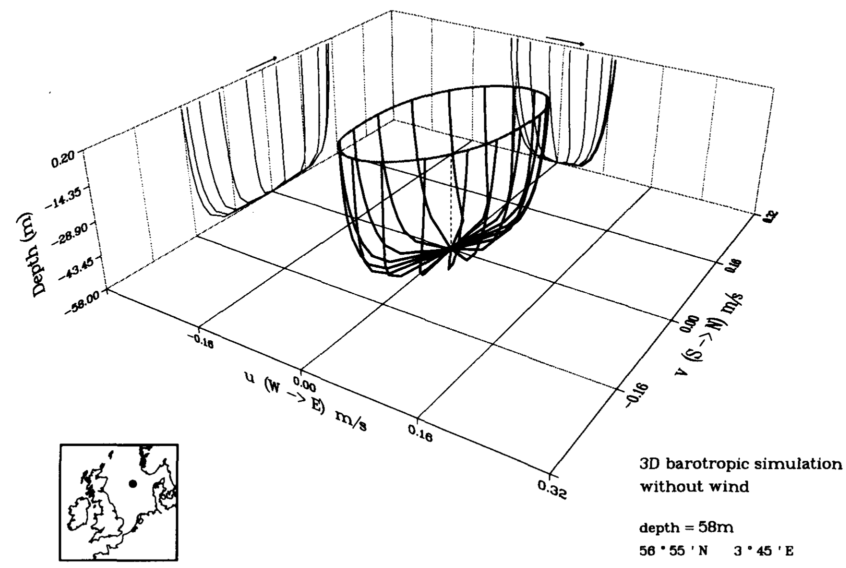

Fig. 5. Evolution of the vertical profile of the horizontal velocity during one M_2 tidal period. Point 2 in the North Sea.

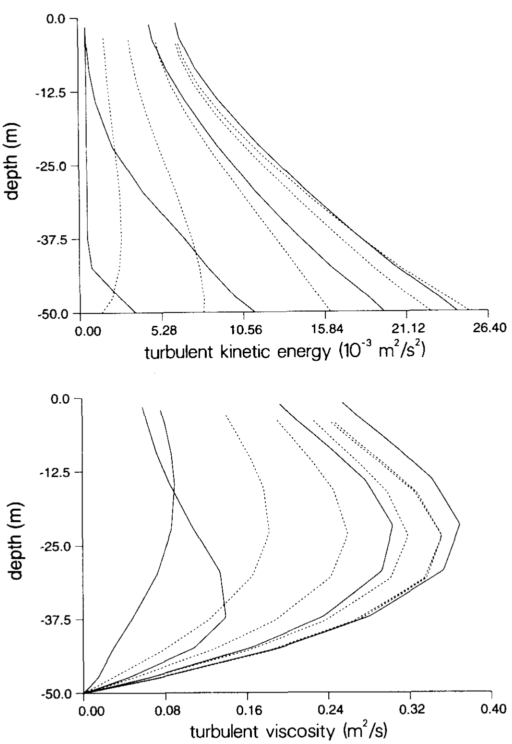

Fig. 6. Evolution of the vertical profiles of the turbulent kinetic energy and the turbulent viscosity at point 1 (English Channel). Barotropic M_2 tide.

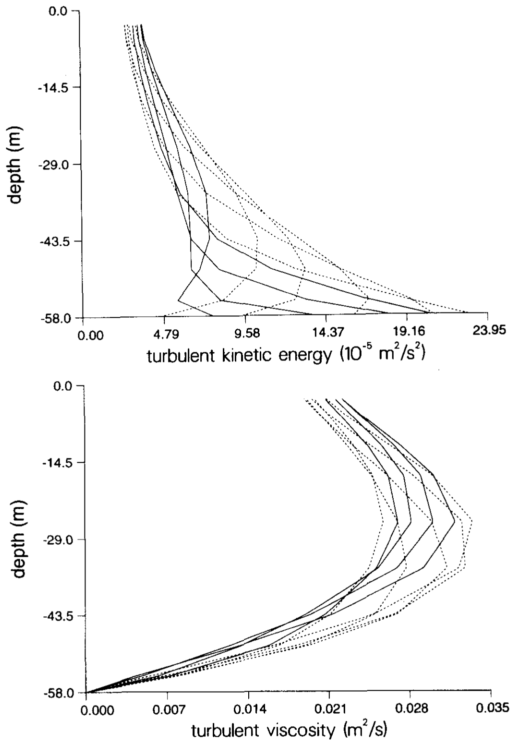

Fig. 7. Evolution of the vertical profiles of the turbulent kinetic energy and the turbulent viscosity at point 2 (North Sea). Barotropic M_2 tide.

energy flux going upwards from the bottom logarithmic boundary layer decreases, the profiles (dotted lines when bottom turbulence decreases, from right to left) become more uniform. This is due to the important vertical diffusion allowed by the high turbulent level reached. The vertical profiles of $\tilde{\nu}$ reflect those of k and of the mixing length l. They exhibit a maximum value at mid-depth where the turbulent transfer is the most efficient since it is achieved through more extended eddies. As a consequence of the two different kinds of k-profiles associated to the increase or the decrease of the turbulent level, the location of the maximum turbulent viscosity undergoes vertical translations along the tidal cycle. When the vertical k-profile is nearly uniform, the maximum $\tilde{\nu}$ is found where the mixing length has its maximum (i.e., a little above mid-depth). On the other hand, when the turbulent level increases, the high value of k found near the bottom makes the maximum turbulent viscosity go down in the water column. Quantitatively, these results show that the turbulent kinetic energy is two orders of magnitude larger in the English Channel (up to $26 \cdot 10^{-3}$ $m^2\,s^{-2}$) than in the central North Sea (only $23 \cdot 10^{-5}\,m^2\,s^{-2}$).

In winter, strong winds blow over the NWECS and generate a sufficient mixing to allow the use of a barotropic model. In a second barotropic simulation using real winter wind forcing (3 hour resolution in time and $\frac{1}{2}°$ resolution in longitude and latitude), we notice a significant intensification of the depth-mean value of the turbulent kinetic energy, time-averaged over 6 M_2 tidal periods (Fig. 8). In the main part of the North Sea, k exceeds $0.5 \cdot 10^{-3}\,m^2\,s^{-2}$ while it doesn't even reach $0.25 \cdot 10^{-3}\,m^2\,s^{-2}$ without wind. In winter, there is a quasi-uniform and high surface value of k due to the turbulence input from strong winds while the bottom distribution remains qualitatively the same with a general intensification. This high turbulent level explains how winter

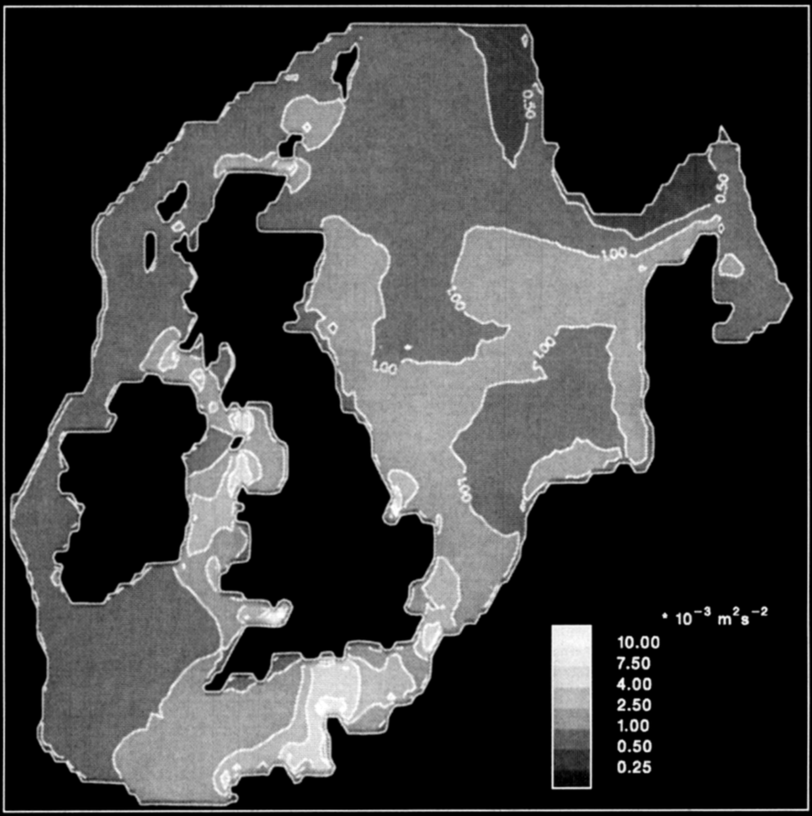

Fig. 8. Depth-mean value of the turbulent kinetic energy. Barotropic results time-averaged over 6 M_2 tidal periods in typical winter conditions.

storm surges ensure a good vertical mixing and how they manage to redistribute remineralized bottom nutrients over the whole water column.

Winter winds affect vertical profiles of k, $\tilde{v}$ and tidal currents. While there is no significant effect in high tidal currents regions (e.g., at point 1 in the English Channel), these modifications are particularly obvious in regions of weak tidal currents (point 2). At this point 2, one can see that the turbulent kinetic energy magnitude increases progressively from bottom to top instead of having its maximum at the bottom (Fig. 9). This is due, in nearly equal proportions, to the important surface flux of turbulence and to the enhanced wind-induced shear at this place where the bottom generated turbulence is rather weak. The bottom value of k oscillates mainly at twice the M_2 tidal frequency while the surface turbulent level reflects the variations of the wind forcing. The turbulent viscosity maximum occurs of course at the surface. Velocity profiles are also strongly affected by winds in this region.

While there is nearly no stratification on the shelf in winter, the NWECS is characterized by frontal structures separating well-mixed waters from stratified ones in summer. Indeed, in spring, the heat input largely concentrated in the surface layer becomes positive. In regions of low tidal mixing, like the main part of the North Sea, a seasonal thermocline develops, separating warm waters in the surface layer from cooler ones beneath. Stratification persists throughout summer. On the other hand, a large part of the shelf is made up of shallow regions where the tidal stirring is sufficient to maintain the vertical homogeneity of the water column all over the year, preventing any stratifica-

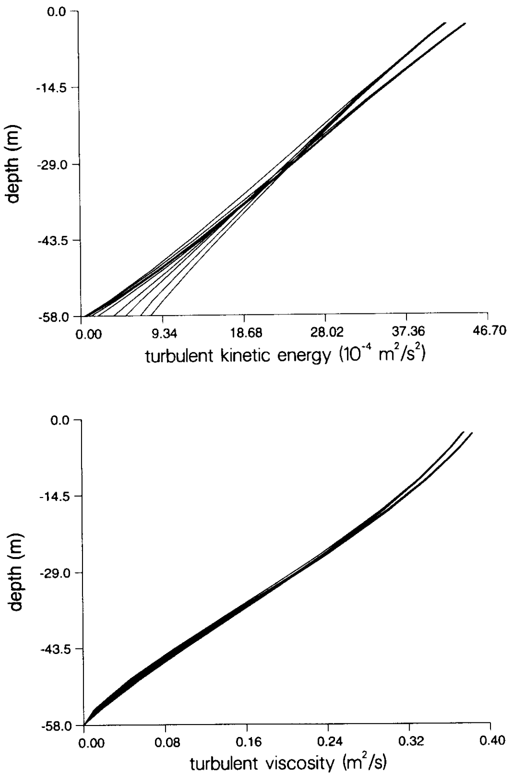

Fig. 9. Evolution of the vertical profiles of the turbulent kinetic energy and the turbulent viscosity at point 2 (North Sea) in typical winter conditions. Barotropic results.

tion to occur. In these regions (e.g., the Eastern English Channel), well-mixed waters exhibit cooler surface temperature than in stratified regions, especially in spring. The average locations of tidal fronts are often predicted from barotropic (even 2D) tidal results, using energy considerations together with empirical analysis (Simpson et al., 1978; Pingree and Griffiths, 1978; Davies and Jones, 1990). Fronts are considered to develop where some energetic ratio (or the turbulent kinetic energy when a 3D barotropic turbulent closure model is used) reaches an empirical critical value. These methods succeed rather well in predicting front locations because spatial variations of the bathymetry and of the tidally induced turbulence explain much of the fronts genesis. This kind of prediction can be made with our 3D barotropic results. Considering Fig. 2, we could locate the transitory zone between well-mixed and stratified regions around the k-contour of $0.25 \cdot 10^{-3}\,\mathrm{m}^{-2}\,\mathrm{s}^{-2}$. However, these methods only predict where fronts are likely to develop and not whether they do exist. The formation of a front will ultimately depend on the occurrence of favourable conditions (mainly meteorological) that can only be appraised with a 3D model computing explicitly the temperature and salinity fields.

A third simulation corresponding to these typical summer conditions has been carried out with the full baroclinic model forced by the M_2 tide and real summer winds (3-h resolution in time and $\frac{1}{2}°$ resolution in longitude and latitude). In order to limit artificial transitory effects, the initial state for this baroclinic simulation is formed by adding the mesoscale barotropic velocities (and elevation) and the residual baroclinic ones obtained through

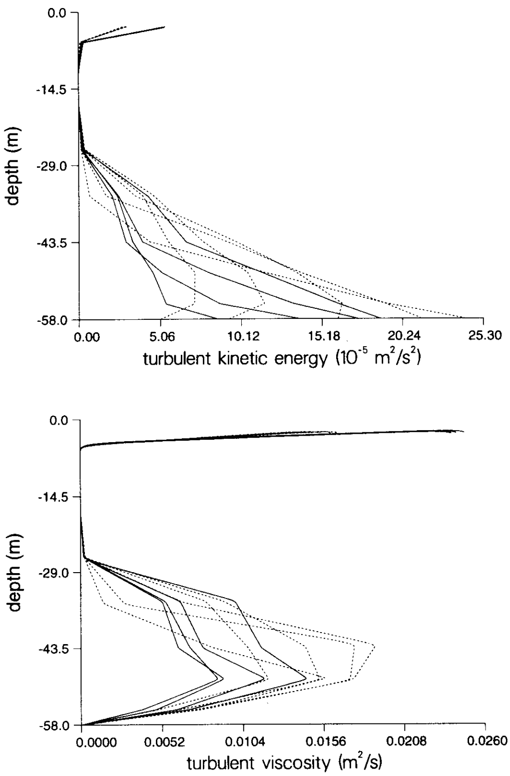

Fig. 10. Evolution of the vertical profiles of the turbulent kinetic energy and the turbulent viscosity at point 2 (North Sea) in typical summer conditions. Baroclinic results.

a separate residual model of the same area (Delhez and Martin, 1992). The initial temperature and salinity fields are those obtained with the same residual model. Temperature and salinity fields are explicitly computed during the mesoscale simulations (eqs. (5) and (6)) to allow their dynamic adjustment and avoid any unphysically persistent baroclinic forcing.

In well-mixed regions, vertical profiles of currents, turbulent kinetic energy or turbulent viscosity are identical to the ones obtained in the barotropic simulation. In these regions the flux Richardson number R_f nearly equals zero and everything looks like as if a barotropic model was used. The weak summer winds, as for them, can't have any noticeable effect in these regions of intense tidal activity.

In stratified regions like the Central North Sea (point 2), the profiles exhibit a threefold structure (Fig. 10). At this point there is a nearly uniform salinity and a step of 5°C between 8 and 30 meters under the surface. In the bottom layer, under the pycnocline, the profiles are similar to the barotropic ones. In the seasonal pycnocline, vertical stratification inhibits turbulence and very low levels of both k and $\tilde{\nu}$ are found. Above, k and $\tilde{\nu}$ increase gradually from the pycnocline to the top because of a turbulence input due to summer winds. Because of the inhibition of vertical turbulent exchanges through the pycnocline and of the smallness of vertical velocities, the top and bottom boundary layers are actually uncoupled in stratified regions. The same uncoupling is found in the vertical profiles of the velocity.

6. Conclusions

Two different sources account for the particularly high turbulent levels reached on the NWECS: the friction of the intense mesoscale currents on the bottom and the drag and waves induced by the wind in the surface layer. The way these sources combine together largely depends on their actual magnitude but also on the local depth and the existence of a stratification inhibiting vertical exchanges. So, at some places, the top and bottom layers merge while in deeper regions the wind and bottom friction dominated layers are distinct and can be clearly separated, possibly by a pycnocline. Our turbulence model turns out to be able to describe both situations.

The analysis of the variations of the turbulent kinetic energy profile during a tidal cycle reveals a large dependence on the tidal ellipse eccentricity. Where the ellipse is linear, turbulence varies a lot during the tidal cycle, while a much more constant level is observed with nearly circular ellipses. Besides, two kinds of k-profiles associated respectively to the increase and the decrease of the turbulent level have been identified.

The lack of turbulence measurements on a large scale prevents us from comparing our results to actual field data. In this context, it seems important to study, at least, the influence of the parameterization on the solution. As a further step, it would thus be very interesting to compare different closure models with respect to their reliability, to the sensitivity of the solution to different sets of parameters, to their respective computer requirements and also to their possible applications and limitations. For example, it seems unnecessarily expensive to use a very complex level $2\frac{1}{2}$ Mellor and Yamada (1982) turbulent closure model to study the free surface motions associated to such a simple barotropic process as the propagation of the tidal wave. Such a phenomenon is already well described by depth-integrated models and should thus exhibit only a weak dependence on the exact formulation of the turbulent closure. On the other hand, a simple algebraic closure cannot be used to solve the problem of the vertical diffusion of a passive constituent, vertical diffusion being then one of the key-processes controlling the exact spatial distribution of this constituent. In this field of the modelization science, as in any other one, a basic principle of modelization must be applied: the complexity of the model must be adapted to the amount of data available for calibration and to the requirements of the application.

7. Acknowledgments

This study would not have been possible without the support of IBM and of the Ministry of Education and Research in the scope of the Program of Concerted Actions (no. 89/94-131). The authors wish also to express their gratitude to the Belgian National Fund for Scientific Research.

REFERENCES

Arakawa, A. and Lamb, V. 1977. Computational design of the basic dynamical processes of the UCLA general circulation model. *Methods in Computational Physics* **17**, 173–265.

Backhaus, J. O. and Hainbucher, D. 1987. A finite difference general circulation model for shelf seas an its application to low frequency variability on the North European shelf. In: *Three-dimensional models of marine and estuarine dynamics* (eds. Nihoul, J. C. J. and Jamart, B.). Elsevier, Amsterdam, 221–244.

Beckers, J. M. 1991. Application of the GHER 3D general circulation model to the Western Mediterranean. *J. Marine Systems* **1**, 315–332.

Blumberg, A. and Mellor, G. 1987. A description of a three-dimensional coastal ocean circulation model. In: *Coastal and estuarine science-4*. AGU publications, Washington, DC, 1–16.

Davies, A. M. and Furnes, G. K. 1980. Observed and computed M_2 tidal currents in the North Sea. *J. Phys. Oceanogr.* **10**, 237–257.

Davies, A. M. and Jones, J. E. 1990. Application of a three-dimensional turbulence energy model to the determination of tidal currents on the Northwest European Shelf. *J. Geophys. Res.* **95**, 18143–18162.

Deleersnijder, E. and Nihoul, J. C. J. 1988. Turbulent fields associated with the general circulation in the Northern Bering Sea. In: *Small-scale turbulence and mixing in the ocean* (eds. Nihoul, J. C. J. and Jamart, B.). Elsevier, Amsterdam, 77–93.

Delhez, E. J. and Martin, G. P. 1992. Preliminary results of 3D baroclinic numerical models of the mesoscale and macroscale circulations on the North-Western European Continental Shelf. *J. Marine Systems* **3**, 423–440.

Flather, R. A. 1976. A tidal model of the North-West European Continental Shelf. *Mem. Soc. Roy. Sc. Liège*, serie **6**, 10, 141–164.

Heaps, N. S. 1983. Storm surges, 1967–1982. *Geophys. J. R. Astr. Soc.* **74**, 331–376.

James, I. D. 1986. A front-resolving sigma coordinate sea model with a simple hybrid advection scheme. *Appl. Math. Modelling* **10**, 87–92.

Leenderste, J. J. and Liu, S. K. 1978. A three-dimensional turbulent energy model for non-homogeneous estuaries and coastal sea systems. In: *Hydrodynamics of estuaries and fjords* (ed. Nihoul, J. C. J.). Elsevier, Amsterdam, 387–405.

Lumley, J. L. 1978. Computational modelling of flows. In: *Advances in applied mechanics* (ed. Yih, C. S.). Academic Press, New York, 18, 123–176.

Mellor, G. L. and Yamada, T. 1982. Development of a turbulence closure model for geophysical fluid problems. *Reviews of geophysics and space physics* **vol. 20**, 4, 851–875.

Nihoul, J. C. J. 1980. *Basic equations of geophysical fluid dynamics and their application to ocean-atmosphere weather and climate models.* Special University Lectures, Department of Mathematics, Imperial College, London. 61 pp.

Nihoul, J. C. J. 1982. *Hydrodynamic models of shallow continental seas. Application to the North Sea.* E. Riga Publ., Liège. 198 pp.

Nihoul, J. C. J. 1984. A 3D general marine circulation model in a remote sensing perspective. *Annales Geophysicae* **2**, 4, 433–442.

Nihoul, J. C. J., Deleersnijder, E. and Djenidi, S. 1989. Modelling the general circulation of shelf seas by 3D $k-\varepsilon$ models. *Earth Science Reviews* **26**, 163–189.

Pingree, R. D. and Griffiths, D. K. 1978. Tidal fronts on the shelf seas around the British Isles. *J. Geophys. Res.* **83**, 4615–4622.

Rodi, W. 1987. Examples of calculation methods for flow and mixing in stratified fluids. *J. Geophys. Res.* **92**, 5305–5328.

Ronday, F. C. 1976. Modèles hydrodynamiques. In: *Modélisation des systèmes marins. Projer Mer, rapport final* (ed. Nihoul, J. C. J.). Service de la politique scientifique, Brussels, vol. 3, 270 pp.

Schwiderski, E. W. 1979. *Global ocean tides, part two: the semi-diurnal principal lunar tide* (M_2). Atlas of tidal charts and maps, Nav. Surf. Weapons Carter rep. (NSWCTR) 79.

Simon, S. T. 1974. Verification of numerical models of Lake Ontario. Part I: Circulation in spring and early summer. *J. Phys. Oceanogr.* **4**, 507–523.

Simpson, J. H., Allen, C. M. and Morris, N. C. 1978. Fronts on the Continental Shelf. *J. Geophys. Res.* **83**, 4607–4614.